Electromechanical Energy Conversion Systems (EECS)
Niroo Research Institute (NRI)
Vol. 4, No. 2, Summer 2025, pp. 66-75
DOI: 10.30503/eecs.2025.504836.1072
Original Article

Torque Ripple Reduction in a Modular Drive of Twelve-Phase, Non-Sinusoidal PMSM with Double Stator Windings based on an Ultra-local model and Extended State Observers (ESO)

Abolfazl Halvaei Niasar*, and Maleki, Davood

Abstract

In the electric drive systems of marine propulsion, particularly in submarines, multiphase permanent magnet synchronous motors (PMSMs) have garnered significant attention due to their enhanced reliability in high-power applications. This paper investigates a twelve-phase non-sinusoidal PMSM with double stator windings, where each stator phase's windings are symmetrically positioned relative to the stator centre. Each winding is powered by a single-phase H-bridge inverter, with both inverters of each phase controlled by a dedicated microcontroller. Given the independent control system for each phase, conventional *dq*-axis modeling and control methods are not applicable. Instead, the system is modeled in a stationary 12-phase reference frame. Furthermore, due to the non-sinusoidal back-EMF voltage waveforms, harmonic current injection is independently applied to each phase to mitigate torque ripple. For harmonic reference current regulation, a state feedback controller based on an ultra-local model is employed, replacing traditional PI or hysteresis controllers. Additionally, extended state observers (ESOs) are designed to estimate uncertainties and parameter mismatches. Simulation results validate the superiority of the proposed control approach.

Keywords: Drive, Twelve-phase PMSM motor with double stator windings, Ultra-local model, Extended state observer, H-bridge inverter, Reliability.

Received Date:2025-02-05; Revised Date: 2025-04-26; Accepted Date: 2025-09-17

1. INTRODUCTION

Permanent Magnet Synchronous Motors (PMSM) are of special interest in high-power submarine systems, due to their high torque and high-power density, smooth torque, considerable efficiency, and higher reliability. Despite the high reliability of three-phase PMSM motors, if a fault occurs in one of the inverter switches or one of the windings, the motor stops developing torque. Therefore, to further increase the reliability of drives, especially in high-power applications, the use of multiphase PMSMs for vehicles such as submarines is highly regarded. Increasing the number of phases reduces phase currents, thereby alleviating the problems of motor losses and cooling [1, 2].

Three-phase PMSMs with double star winding (or asymmetric six-phase) are used in low to medium power applications, while twelve-phase PMSMs are used in high power applications. Fig. 1 shows various types of electric drives for twelve-phase PMSMs (and more generally multiphase motor drives). Multiphase motors are divided into symmetric and asymmetric categories [3]. In symmetric multiphase PMSM motors such as five-phase and seven-phase motors, the number of phases is often an odd number. Asymmetric multiphase motors usually include two or more sets of three-phase windings and are spatially asymmetric. Six-phase and twelve-phase motors fall into this category, comprising two sets of three-phase windings and four sets of three-phase windings, respectively. Assuming N ($N = 2,3,\dots$) sets of asymmetric three-phase windings are employed, the angle β between two identical windings in different sets is $(3N)/\pi$. These motors offer greater reliability compared to symmetric multiphase motors, which, with each set of three phases, can be fed by a separate three-phase frequency inverter.

Fig. $1(a)$ shows a twelve-phase motor with a single star connection point, powered by a twelve-phase inverter. Fig. $1(b)$ shows a twelve-phase motor, with each phase powered by an independent single-phase inverter. Fig. $1(c)$ shows a

Faculty of Electrical and Computer Engineering, University of Kashan
**Corresponding author, Email: halvaei@kashanu.ac.ir*

twelve-phase PMSM with four sets of three-phase windings, having only one star connection point, powered by four independent three-phase inverters. Fig. $1(d)$ shows a twelve-phase PMSM with four sets of three-phase windings, each with four separate star points, powered by four independent three-phase inverters.

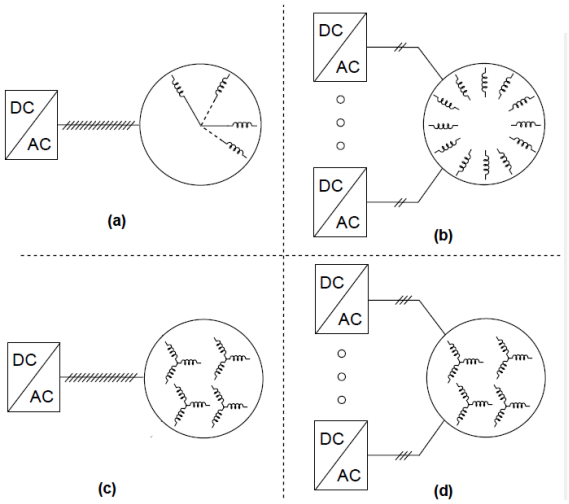

Fig. 1. Various types of electrical drives for 12-phase PMSM [3]

Scheme (a) of a twelve-phase PMSM motor drive fed by a single twelve-phase inverter is generally not used because a single short-circuit fault in one of the twelve inverter legs causes a complete phase shutdown. Schemes (c) and (d) are common twelve-phase PMSM motor drive schemes that use four independent three-phase inverters. In these two schemes, the motor has four sets of symmetrical three-phase windings, where the corresponding windings of different three phases are spatially separated by 15 degrees. Fig. 2 shows the winding axis configuration of scheme (c), where the four sets of three-phase windings share a common star point, and this scheme is more commonly used than scheme (d) [4]. Fig. 3 shows the schematic of the drive system for this twelve-phase PMSM scheme [5].

Scheme (b) has the highest level of reliability because each motor phase is independently fed by a single-phase H-bridge inverter. With failure in one of the windings or an H-bridge inverter, the remaining 11 phases of the motor continue to develop torque [6]. This structure is popularly designed and implemented. One of the features of this scheme is too many numbers of switches, totaling 48, which is twice the number of switches in the drive system shown in Fig. 3. A limitation of this method is that, due to the modular nature of the control system, there is no electrical communication between the drive systems of different phases, and the controllers of different modules are unaware of each other's voltage and current data.

In this paper, due to the demanded high reliability, a design similar to the modular scheme (b) is used, where each phase has two windings, referred to as a double twelve-phase motor. In the design shown in Fig. 4, the windings are distributed at 15-degree angles relative to each other. Each half of a motor phase is located within a 180-degree range of the stator perimeter, and the second half of each phase winding with the first half is aligned, but on the opposite side of the stator. It should be noted that this motor essentially has 24 independent single-phase H-bridge inverters and a total of 96 IGBTs, controlled by 12 independent microcontrollers. Fig. 5 displays the schematic of the modular drive for the double winding twelve-phase PMSM, where each half of a phase winding is fed by a single-phase H-bridge inverter. At low speeds, to increase motor efficiency, the two parts of each phase winding are connected in series, and by deactivating one leg of the H-bridge inverter related to each half, the entire phase winding is powered by one H-bridge. According to Fig. 5, both H-bridge inverters for a phase are controlled by a common microcontroller. It has no data sharing with other microcontrollers, and a central microcontroller determines the phase reference currents and monitors the phase status to change the reference current in case of any fault.

Symmetrical three-phase PMSMs with sinusoidal back-EMF voltage are usually modeled in the rotating dqreference frame and controlled using vector control methods. Similar to three-phase PMSMs, there are four modeling methods for multiphase PMSMs [7, 8]:

- Modeling in multiple dq reference frames
- Modeling in decoupled dq reference frames
- Modeling using vector space decomposition
- Modeling in multiple stationary reference frames

Due to the modular structure of the drive used in this paper, where the local microcontrollers of each three-phase group are blind to the other groups, modeling methods based on the dq reference frame cannot be used. Moreover, if the back-EMF voltages of PMSM were not sinusoidal and include higher harmonics, the use of the Park transform for modeling cannot adequately represent the motor behavior. Several methods have been proposed for modeling of non-sinusoidal PMSM, including:

- Modeling based on the extended Park transform [9]
- dq modeling with harmonic components [10]
- Modeling in multiple dq reference frames [11]
- Vector space decomposition (VSD) [12]

The above-mentioned methods for modeling non-sinusoidal three-phase PMSMs have a significant computational volume. Furthermore, using these methods for a twelve-phase motor, the computational volume increases several times. Also, as shown in Fig. 5, the control calculations of each phase are performed in the local microcontroller itself. Therefore, it is not possible to perform 3-to-2 transformations and vice versa. Thus, for the twelve-phase PMSM with a modular structure and non-sinusoidal back-EMF voltages, modeling in the dq reference

frame is not possible. So, modeling in twelve-axis stationary reference frames must necessarily be used, in which the angle between two adjacent windings is equal to 15 electrical degrees. Of course, modeling in a stationary reference frame is feasible for surface-mounted PMSM, where the self-inductances and mutual inductances are constant.

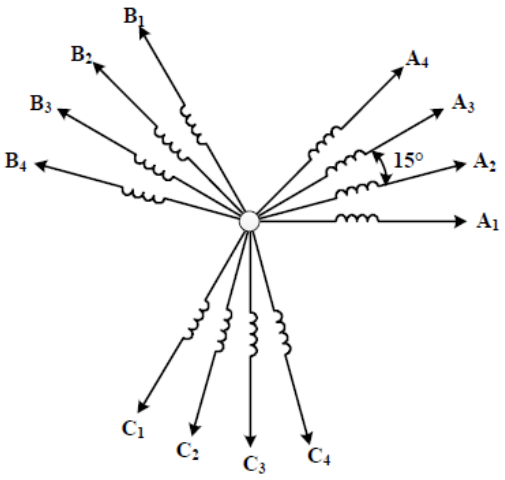

Fig. 2. Four-star connected asymmetric 12-phase PMSM windings distribution [5]

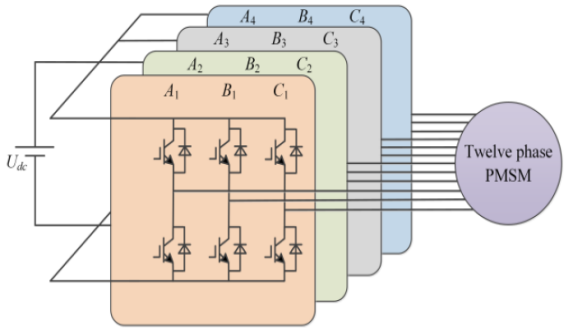

Fig. 3. The topology of a 12-phase PMSM drive fed by four three-phase inverters [5]

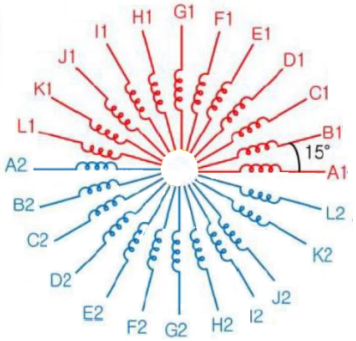

Fig. 4. Open-end connected symmetric 12-phase PMSM with double winding distribution.

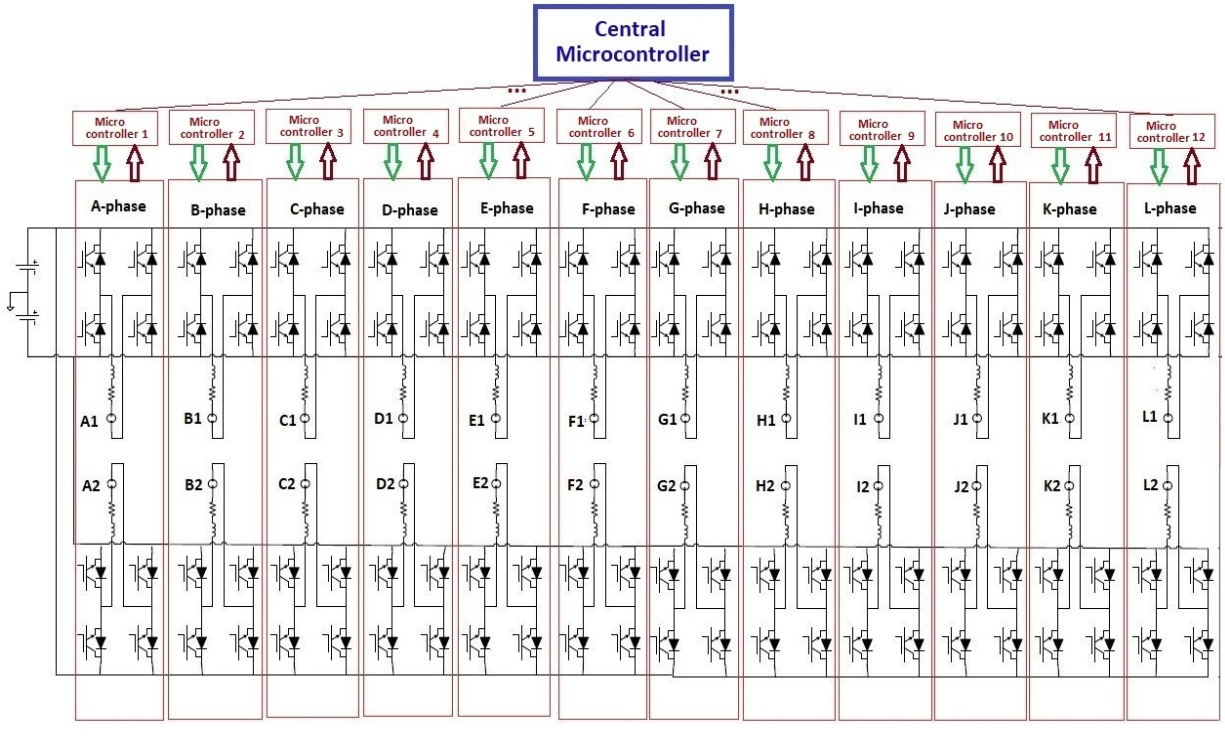

Fig. 5. Schematic of the modular drive system for the 12-phase PMSM with double winding studied in this paper

Due to the independence of the microcontrollers and the absence of data exchange between them, the use of *dq* transformations is not feasible. As a result, many modeling and estimation methods based on the multiple *dq*-axis theory cannot be applied. Furthermore, common control strategies such as field-oriented control (FOC), model predictive control (MPC), and direct torque control (DTC) are impractical for this system. Additionally, the non-sinusoidal back-EMF voltages of the motor prevent the use of traditional sinusoidal PMSM control methods, as they would introduce significant torque ripple. To address these challenges, this multi-phase PMSM is modeled in a 12-axis stationary reference frame. Moreover, a current shaping method—based on harmonic current injection—is employed to mitigate torque ripple caused by the non-sinusoidal back-EMF waveforms. So, the innovation of this paper includes the use of a harmonic current injection method to reduce the torque ripple of a double twelve-phase motor and the development of an extended state observer for robust control of this motor.

In the rest of this paper, Section 2 presents the modeling of the double-winding twelve-phase PMSM, considering the limitations of the modular system. Section 2 discusses the drive control with respect to non-sinusoidal back-EMF voltages, using the harmonic current injection method. In section 3, the mathematical modeling based on the ultra-local model is presented and then, an extended state observer (ESO) is designed in the stationary six-axis reference frame for current regulation. Section 4 provides the simulation results for verifying the proposed method, followed by a conclusion in Section 5.

2. Modeling of Modular Twelve-Phase PMSM

Assuming the winding arrangement of the phases of the PMSM is as shown in Fig. 4, the voltage-current relationship of each winding obeys the following:

$$v_x = R_s i_x + \frac{d}{dt}\psi_x + e_x \tag{1}$$

where, R_s is the resistance of each winding, and v_x, i_x, ψ_x and e_x are the voltage, current, flux linkage and back-EMF voltage due to the rotor flux of the xth winding, respectively, that $x = A_1, A_2, B_1, B_2, \dots, L_2$. The flux linkage of each winding depends on the itself current and the current of the other 23 windings, and can be calculated as follows:

$$\psi_x = L_x i_x + \sum_{\substack{y=A_1,A_2,B_1,B_2,\dots,L_2 \\ (x\neq y)}} M_{xy} i_y \tag{2}$$

where L_x and M_{xy} are the self-inductance of winding x and the mutual inductance between the two windings x and y respectively. The electromagnetic torque of the double twelve-phase motor (T_e) and the mechanical speed of the motor (ω_m) can also be calculated from the following relations:

$$T_e = \sum_{x=A_1,\dots,L_2} \frac{e_x i_x}{\omega_r} \tag{3}$$

$$\omega_m = \frac{1}{J}\int (T_e - T_l)dt \tag{4}$$

where, ω_r, J, and T_l are the rotor electrical speed, the total moment of inertia of the rotor and the load torque, respectively. To implement the motor model in Simulink, a 24-phase winding can be used, where each winding is considered in series with a speed-dependent voltage source e_x with as well as an arbitrary harmonic waveform depending on the rotor position θ_r.

3. Control of Modular Twelve-Phase PMSM Using Harmonic Current Injection Method

In the harmonic current injection method, considering the harmonics in the phase's back-EMF voltage, harmonic currents are injected in each phase, in which their amplitude are adjusted in such a way that the harmonic components of the torque become zero and only the constant torque remains [13,14]. For the motor studied in this paper, it is assumed that only harmonics 1, 3, 5, and 7 are present in the back-EMF voltages. Hence, the back-EMF voltage of winding x can be written as follows:

$$e_x(t) = E_1 \sin \omega_r t + E_3 \sin 3\,\omega_r t + E_5 \sin 5\,\omega_r t + E_7 \sin 7\,\omega_r t \tag{5}$$

where $x = A_1, A_2, B_1, B_2, \dots, L_2$, and E_1 to E_7 are the harmonics amplitudes of back-EMF voltages, that in this paper are equal to 1, 0.2, 0.1, and 0.02 in terms of per unit, respectively. If the current injected into coil x is considered as follows:

$$i_x(t) = I_1 \sin \omega_r t + I_5 \sin 5\,\omega_r t + I_7 \sin 7\,\omega_r t \tag{6}$$

Note that the above back-EMF voltage and current equations belong to winding $x = A_1$. For other windings, the argument of the sinusoidal functions is considered according to Fig. 4. For example, for winding B_1, 15^o is added to the argument $\omega_r t$ in all sinusoidal functions, and for winding L_1, 165^o is added. The air gap power of winding x will only include even harmonics up to order 14 and will be as follows:

$$P_x(t) = P_0 + P_2 \sin 2\omega_r t + \dots + P_{14} \sin 14\,\omega_r t \tag{7}$$

It can be easily shown that the air gap power or torque of the sum of all windings in a PMSM with a number of phases equal to a multiple of 3, only has harmonics with multiples of 6. By limiting the harmonics to order 7, for the motor of

this paper, the instantaneous air gap power P_e is obtained as follows:

$$P_e(t) = P_0 + P_6 \sin 6\omega_r t + P_{12} \sin 12\,\omega_r t \quad (8)$$

and the instantaneous electromagnetic torque can also be calculated as:

$$T_e(t) = \frac{P_e(t)}{\omega_r} = T_0 + T_6 \sin 6\omega_r t + T_{12} \sin 12\,\omega_r t \quad (9)$$

where

$$T_0 = \frac{3}{2\omega_r}[E_1 I_1 + E_5 I_5 + E_7 I_7] \quad (10)$$

$$T_6 = \frac{3}{2\omega_r}[I_1(E_7 - E_5) - I_5 E_1 + I_7 E_1] \quad (11)$$

$$T_{12} = \frac{3}{2\omega_r}[-I_5 E_7 - I_7 E_5] \quad (12)$$

To determine the amplitude of current harmonics, by equating the value of T_0 to the reference torque T_e^* (speed controller output) and setting T_6 and T_{12} to zero, the following matrix equation must be solved:

$$\begin{bmatrix} E_1 & E_5 & E_7 \\ E_7 - E_5 & -E_1 & E_1 \\ 0 & -E_7 & -E_5 \end{bmatrix} \times \begin{bmatrix} I_1 \\ I_5 \\ I_7 \end{bmatrix} = \frac{2\omega_r}{3} \begin{bmatrix} T_e^* \\ 0 \\ 0 \end{bmatrix} \quad (13)$$

As a result, the reference values of the harmonic currents will be determined as follows:

$$\begin{bmatrix} I_1^* \\ I_5^* \\ I_7^* \end{bmatrix} = \begin{bmatrix} 1.006 \\ -0.0671 \\ 0.0134 \end{bmatrix} \frac{2\omega_r T_e^*}{3} \quad (14)$$

Note, the reference value of the third harmonic current is considered to be zero, because this harmonic has no involvement in torque generation.

Using (6) and (14), the time domain of the reference current for both windings of the phase $\boldsymbol{A}$, based on the reference torque (output of the PI speed controller), can be displayed as follows:

$$i_A^*(t) = I_1^* \sin \omega_r t + I_3^* \sin 3\,\omega_r t + I_5^* \sin 5\,\omega_r t \quad (15)$$

The current of phase A windings, in all transient and steady states, must accurately track this harmonic reference value. For this purpose, appropriate current regulators should be employed. The simplest type of current regulator is the hysteresis controller, which, due to its steady-state error of current and high, variable switching frequency, is not suitable for high power applications due to propagated acoustic noise. On the other hand, the simple and traditional PI controller is also not suitable for this application because, due to its small bandwidth, the PI controller is not capable of tracking AC signals containing high-order harmonics [15]. Another solution for tracking harmonic reference signals is the use of proportional-resonant (PR) controllers or quasi-PR (QPR) controllers. The transfer function of the harmonic QPR controller for the harmonic reference current given by relation (15) is as follows:

$$\boldsymbol{G_{QPR,H}(s) = K_P + K_{R_1} \frac{2\omega_{c_1} s}{s^2 + 2\omega_{c_1} s + {\omega_o}^2} + K_{R_3} \frac{2\omega_{c_3} s}{s^2 + 2\omega_{c_3} s + (3\omega_o)^2} + K_{R_5} \frac{2\omega_{c_5} s}{s^2 + 2\omega_{c_5} s + (5\omega_o)^2}} \quad (16)$$

In which the coefficients K_P, K_{R_1}, K_{R_3}, K_{R_5} and the cut-off frequencies $\omega_{c_1}, \omega_{c_3}, \omega_{c_5}$, must be accurately adjusted [16].

As can be seen, the number of adjustable parameters of the harmonic QPR controller is too and their adjustment requires experience or the use of complex design methods in the time or frequency domain. Therefore, to avoid these problems, a simple state feedback controller based on an extended state observer (ESO) is used to regulate harmonic currents such as (15).

4. CURRENT CONTROL OF TWELVE-PHASE PMSM BASED ON EXTENDED STATE OBSERVER (ESO)

In this section, an ultra-local model of the twelve-phase PMSM is first developed. To track the harmonic current references made by the harmonic current injection strategy, a first-order state feedback controller is applied to each winding independently. Due to the nonlinear model and uncertainties of the model, an extended state observer is designed and employed in state feedback controllers.

4.1. Ultra-local mathematical model theory

An ultra-local model of a single-input, single-output system using only the system's input and output while disregarding the mathematical model can be expressed as [17].

$$\dot{y} = \alpha u + F \quad (17)$$

where, $\boldsymbol{y}$ is the output of the system, $\boldsymbol{u}$ is the input of the system, $\boldsymbol{F}$ is the sum of known and unknown disturbances of the system as an extended state, and $\boldsymbol{\alpha}$ is a scaling coefficient of the designed model. Considering $\boldsymbol{y}^*$ as the reference output value of the system, $\widehat{\boldsymbol{F}}$ as the estimated value of $\boldsymbol{F}$, the control law of the state feedback controller can be expressed as:

$$u = \frac{\dot{y}^* - \hat{F} + \xi}{\alpha} \quad (18)$$

here, ξ is the control law and can be the output of a controller such as proportional-integral (PI). If extended state $\boldsymbol{F}$ is estimated with high accuracy, then $\widehat{\boldsymbol{F}} \cong \boldsymbol{F}$, from (17) and (18) it results

$$\dot{e} + \xi = 0 \tag{19}$$

where $\boldsymbol{e} = \boldsymbol{y}^* - \boldsymbol{y}$ represents the output tracking error. Assuming that $\boldsymbol{\xi}$, the output of the proportional controller, is in the form $\boldsymbol{\xi} = \boldsymbol{k_p e}$, the control law of the closed-loop nonlinear system is described as follows:

$$u = \frac{\dot{y}^* - \hat{F} + k_p e}{\alpha}$$
$$\dot{e} + k_p e = 0 \tag{20}$$

It is clear that the performance of the controller depends on the proportional controller coefficient ($\boldsymbol{k_p}$) and the accuracy of the estimation.

4.2. Ultra-local model construction of a twelve-phase PMSM

To develop the ultra-local mathematical model of the modular double-winding, twelve-phase PMSM in the stationary stator frame, the following steps are taken. By rewriting (1) and using (2) for a considered winding such as winding $\boldsymbol{A_1}$ of phase A, it results:

$$v_{A_1} = R_s i_{A_1} + \frac{d}{dt}\psi_{A_1} + e_{A_1} \tag{21}$$

or

$$v_{A_1} = R_s i_{A_1} + L_s \frac{di_{A_1}}{dt} + \frac{d}{dt}\sum_{x_j = B_1 \ldots Z_2} M_{A_1 x_j} i_{x_j} + \omega_r \psi_{PM} \sin(\theta_r) \tag{22}$$

It is observed that, in (22), the voltage of winding $\boldsymbol{A_1}$ depends on the currents of other windings. However, given the modular nature of the power and control system, their values are not available, and the induced voltage due to the currents of other windings can be considered the unmodeled dynamics of the winding $\boldsymbol{A_1}$. Considering parameter variations, unknown disturbances, and unmodeled dynamics, the mathematical model of winding $\boldsymbol{A_1}$ can be expressed as follows:

$$v_{A_1} = (R_s + \Delta R) i_{A_1} + (L_s + \Delta L)\frac{di_{A_1}}{dt} + \omega_r(\psi_{PM} + \Delta\psi_{PM})\sin(\theta_r) + f_{A_1} \tag{23}$$

that, ΔR, ΔL, and $\boldsymbol{\psi_{PM}}$ represent the resistance, inductance and permanent magnet flux variations of each phase, and $\boldsymbol{f_{A1}}$ indicates the unknown disturbances and unmodeled dynamics in phase $\boldsymbol{A_1}$. Equation (23) can be rewritten as follows:

$$\frac{di_{A_1}}{dt} = \frac{v_{A_1}}{L_s} + \left(-\frac{(R_s + \Delta R) i_{A_1}}{L_s} - \frac{\Delta L}{L_s}\frac{di_{A_1}}{dt} - \frac{\omega_r(\psi_{PM} + \Delta\psi_{PM})\sin(\theta_r)}{L_s} - \frac{f_{A_1}}{L_s} \right) \tag{24}$$

If the currents of each of the 24 windings of the motor are considered the system outputs, the applied voltages to the motor windings are considered the system inputs, and the other terms are considered the sum of the known and unknown disturbances of the system. Based on (17), the ultra-local mathematical model for winding $\boldsymbol{A_1}$ PMSM can be expressed as follows:

$$\frac{di_{A_1}}{dt} = \alpha v_{A_1} + F_{A_1} \tag{25}$$

where α is the controller coefficient equal to the inverse of phase inductance ($\alpha = 1/\boldsymbol{L_s}$), and the sum of the disturbances for winding $\boldsymbol{A_1}$ is as follows:

$$F_{A_1} = -\frac{(R_s + \Delta R) i_{A_1}}{L_s} - \frac{\Delta L}{L_s}\frac{di_{A_1}}{dt} - \frac{\omega_r(\psi_{PM} + \Delta\psi_{PM})\sin(\theta_r)}{L_s} - \frac{f_{A_1}}{L_s} \tag{26}$$

For other windings, the ultra-local mathematical model can also be presented in the same manner. In the next section, an ESO is designed for each winding to estimate the sum of the disturbances $\boldsymbol{F_{A_1}}$.

4.3. Design of extended state observer (ESO)

Based on the ultra-local model given by (25), a linear extended state observer can be designed, with the state variables estimating the values of $\boldsymbol{i_{A1}}$ and $\boldsymbol{F_{A1}}$. This observer can be designed using the feedback of the estimation error of the current $\boldsymbol{i_{A1}}$ as follows [30, 29]:

$$\begin{cases} e = x_1 - i_{A_1} \\ \dot{x}_1 = x_2 + \alpha v_{A_1} - \beta_1 \times e \\ \dot{x}_2 = -\beta_2 \times e \end{cases} \tag{27}$$

where $\boldsymbol{x_1} = \hat{\boldsymbol{i}}_{\boldsymbol{A_1}}$ ،$\boldsymbol{x_2} = \widehat{\boldsymbol{F}}_{\boldsymbol{A_1}}$ are the state variables of the observer, those are the estimated values $\boldsymbol{i_{A1}}$ and $\boldsymbol{F_{A1}}$, respectively. $\boldsymbol{\beta_1}$ and $\boldsymbol{\beta_2}$ are the feedback gains of the observer's error, which influence the estimation quality and must be appropriately determined. To design the observer and determine the appropriate values for $\boldsymbol{\beta_1}$ and $\boldsymbol{\beta_1}$, the state-space representation of the linear ESO can be expressed as follows:

$$\begin{cases} \dot{x} = Ax + Bv_{A_1} + D(y - \hat{y}) \\ \hat{y} = Cx \end{cases} \tag{28}$$

that $\hat{\boldsymbol{y}}$ is the estimated output y, and the vector x and observer matrices are as follows:

$$x = \begin{bmatrix} x_1 \\ x_2 \end{bmatrix}, A = \begin{bmatrix} 0 & 1 \\ 0 & 0 \end{bmatrix}, B = \begin{bmatrix} \alpha \\ 0 \end{bmatrix}, C^T = \begin{bmatrix} 1 \\ 0 \end{bmatrix}, D = \begin{bmatrix} \beta_1 \\ \beta_2 \end{bmatrix} \tag{29}$$

The characteristic equation of the ESO observer is expressed as follows:

$$|sI-(A-DC)| = s^2 + \beta_1 s + \beta_2 \tag{30}$$

For stability of the ESO, the roots of the (30) must be located in the left half of the complex plane. Hence, the following conditions must be met:

$$\begin{cases} \beta_1 = 2\omega_0 \\ \beta_2 = \omega_0^2 \end{cases} \tag{31}$$

The bandwidth $\boldsymbol{\omega_0}$ of the ESO determines the stability and dynamic performance of the observer.

For PMSM drives, the current control loop (inner loop) typically requires a high bandwidth to meet dynamic response requirements. Thus, in this paper, when the sampling frequency is 8 kHz, $\boldsymbol{\omega_0}$ is set to 1600 and for higher sampling frequencies, such as 16 kHz, $\boldsymbol{\omega_0}$ is 3200.

4.4. Current regulation using ESO

The relationship between voltage and current for each winding of the motor follows a first-order ultra-local model such (26). Using the Euler discretization approximation, the voltage of motor winding $\boldsymbol{A_1}$ can be calculated as follows:

$$v_{A_1}(k) = \frac{i_{A_1}(k+1) - i_{A_1}(k)}{\alpha T_s} - \frac{\hat{F}_{A_1}(k)}{\alpha} \tag{32}$$

where $\boldsymbol{F_{A_1}}$ is replaced by $\boldsymbol{\hat{F}_{A_1}}$, that is determined by the ESO. By substituting $\boldsymbol{i_{A_1}(k+1)}$ with the reference current of the phase A winding, i.e., $\boldsymbol{i_A^*}$ determined by (15), the reference voltage value of the motor winding $\boldsymbol{A_1}$ is obtained as follows:

$$v_{A_1}^*(k) = \frac{i_A^*(k) - i_{A_1}(k)}{\alpha T_s} - \frac{\hat{F}_{A_1}(k)}{\alpha} \tag{33}$$

By modulating this voltage vector using fixed switching frequency modulation methods such as space vector modulation (SVM) or sinusoidal modulation, the switching signals for each H-bridge inverter shown in Fig. 5 are determined.

5. Simulation Results

In this section, the performance of the proposed control method is validated by performing several simulations. The specifications of the target double-winding, 12-phase PMSM are: 200 kW, 2000 N.m, 300, 320 rpm, stator resistance 15 mΩ, self-inductance 500 µH, and back EMF constant 1.37 V's/rad.

At first, the drive performance is compared using two control strategies: field-oriented control (FOC) and the proposed harmonic current injection (HCI). Fig. 6 shows the results while the FOC strategy is employed in a stationery reference frame. As shown, the current reference is sinusoidal and the phase current tracks the reference current with some high-frequency fluctuations. The torque ripple resulted from non-sinusoidal back-EMFs is considerable and about 300 N.m or 15%. Fig. 7 shows the results of employing HCI strategy. It is evident that the reference current has harmonic with orders 5 and 7 that cancels the effects of non-sinusoidal back-EMFs. Hence, the peak-to-peak torque ripple is reduced to 80 N.m or 4%.

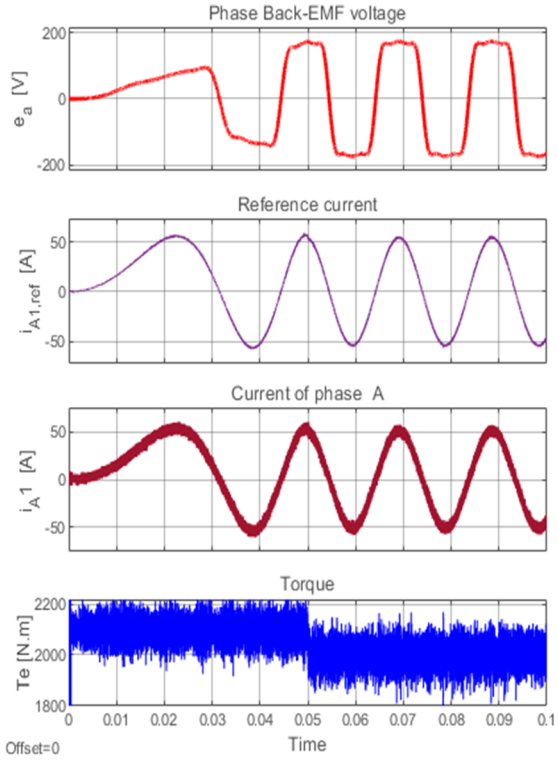

Fig. 6. Drive behavior using field-oriented control (FOC) strategy.

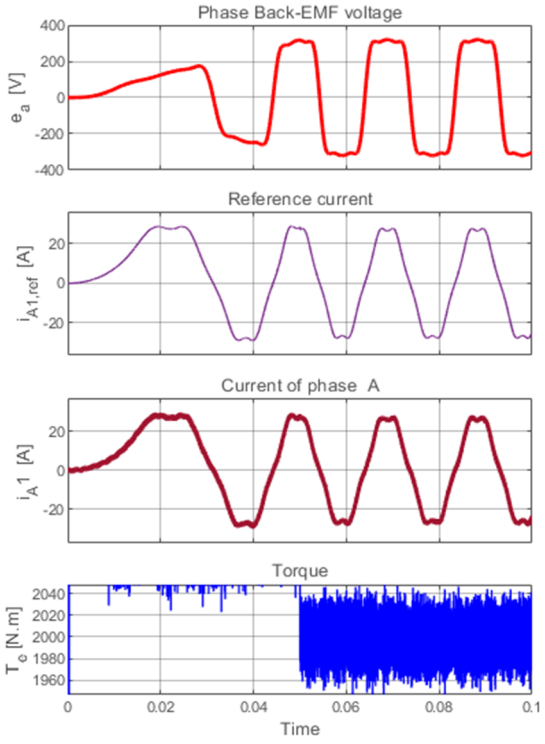

Fig. 7. Drive behavior using harmonic current injection (HCI) strategy

In the continuation of work, motor drive behavior is simulated using a harmonic current injection control strategy and using three types of current regulators: PI, hysteresis, and ESO-based state feedback. Fig. 8 and Fig. 9 show the dynamic response of the 12-phase PMSM drive while using PI and hysteresis regulators, respectively. They are including back EMF of phase A, reference and phase currents of winding A_1, three-winding currents. i_{A1}, i_{G1}, and i_{L1} and electromagnetic torque. It is observed that due to the non-sinusoidal back EMF of the windings, the reference current is harmonic. In Fig. 8, the reference current tracking is carried out well, but some torque ripple occurs due to the limited bandwidth of PI controllers. With a load torque 2000 N.m, the torque ripple is about 300 N.m or 15%. In Fig. 9 and with a hysteresis current regulator, the torque ripple is 100 N.m or 5%. It is noted that the hysteresis band is adjusted in 2 A in a manner that the maximum switching frequency is limited to 16 kHz. Fig. 10 shows the result of employing ESO-based controller. The torque ripple is less while the hysteresis regulator is used and it is reduced to 60 N.M or 3%. Fig. 11 shows the speed tracking and current tracking with ESO-based current controllers. Table 1 compares the numerical values of peak-to-peak torque ripple for each of the three current regulators.

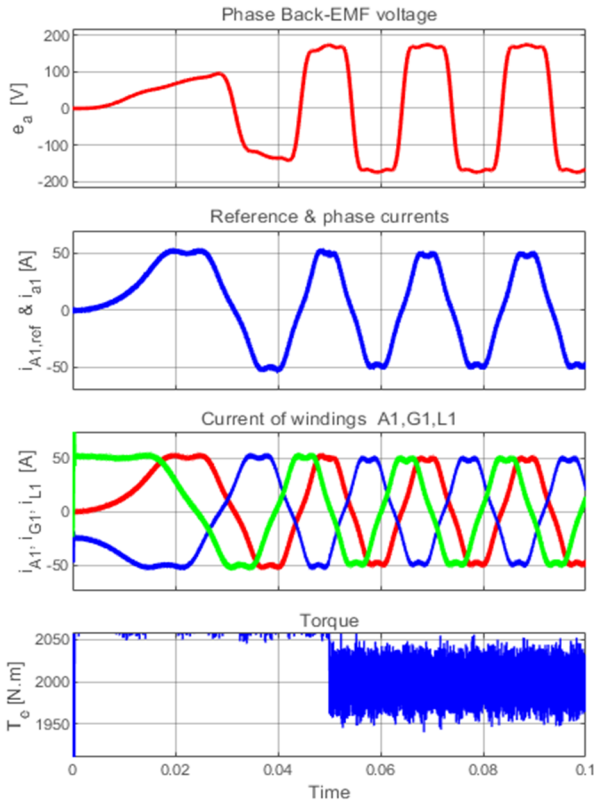

Fig. 9. Drive behavior using hysteresis current controllers

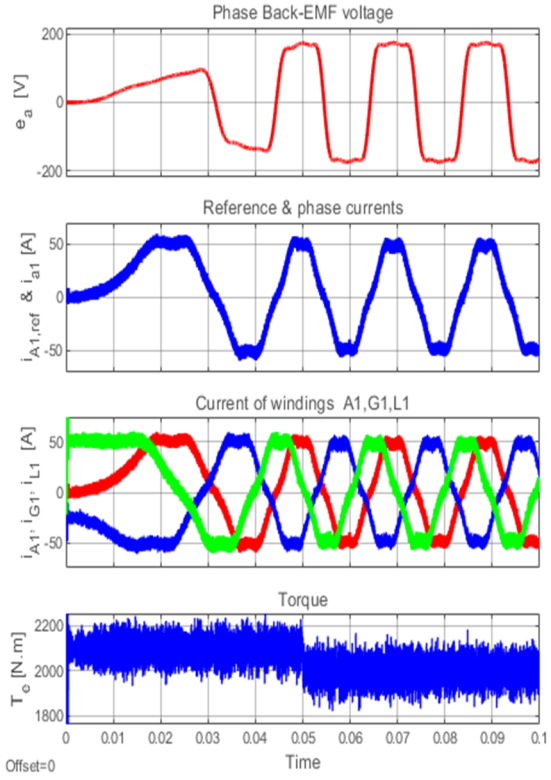

Fig. 8. Drive behavior using PI current controllers

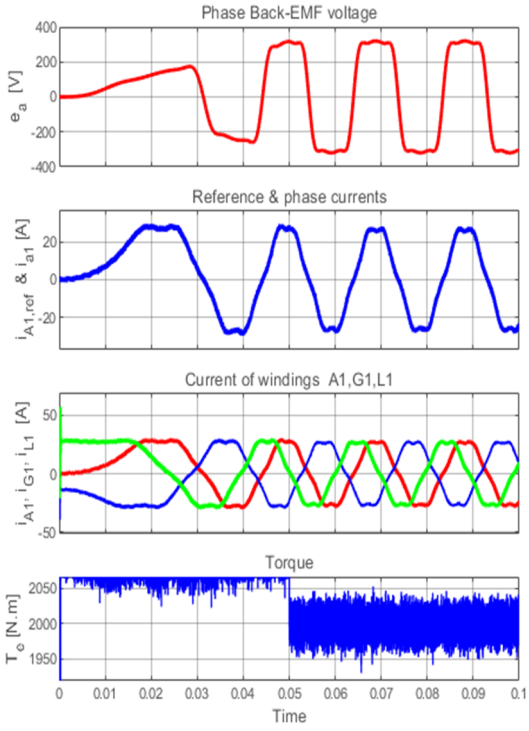

Fig. 10. Drive behavior using ESO based state feedback controllers

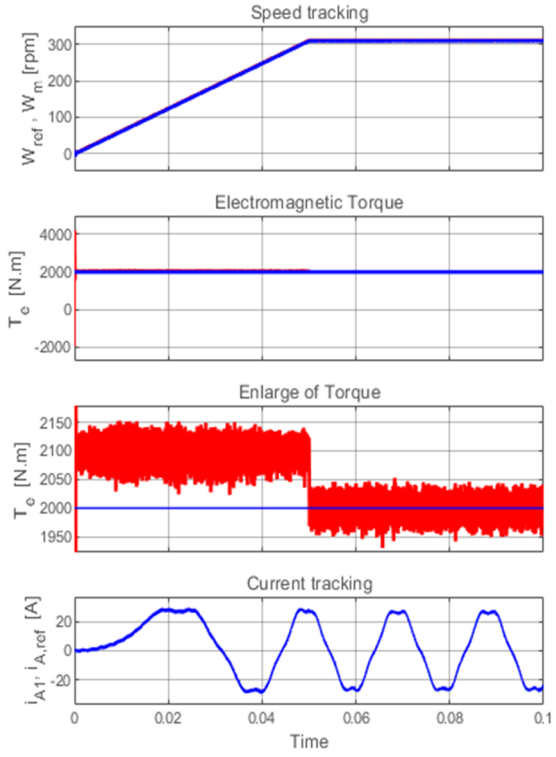

Fig. 11. Speed and current tracking using ESO-based state feedback controllers

TABLE 1. Comparison of the drive behavior of a twelve-phase PMSM motor using the harmonic current injection control method with different current controllers

Controller Type	Torque Ripple (%)
PI	15
Hysteresis	5
ESO-based state feedback	3

6. CONCLUSION

In this paper, the torque ripple reduction of a non-sinusoidal twelve-phase modular PMSM with double stator windings was studied using a novel strategy. Due to the independence of each phase control system from the other phases, the motor modeling was performed in the 12-phase stationary reference frame. Additionally, to control the motor and reduce the torque ripple caused by the non-sinusoidal back-EMF voltages, the reference current shaping method or the harmonic current injection method was employed. Current regulation was carried out using a simple current feedback controller based on an ESO, that the resulted torque ripple was 3%, which shows much better performance than the 15% torque ripple of the PI controller and better than hysteresis and PR. The proposed ESO is robust against variations in the model and uncertainties. The simulation results indicate the capability of the proposed modeling and harmonic current injection with ESO-based current controllers for this special modular drive.

REFERENCES

[1] Kanturska, D. S., "Features in the selection and operation of AC motors for electric propulsion system in ship", 15th International Conference on Electrical Machines, Drives and Power Systems (ELMA), 2017.

[2] Reusser, C. A., Young, H. A., Osses, J. R. P., Perez, M. A., Simmonds, O. J., "Power Electronics and Drives: Applications to Modern Ship Propulsion Systems", IEEE Industrial Electronics Magazine, vol. 14, no. 4, pp. 106-122, 2020.

[3] Benatti, D., Alosa, C., Carfagna, E., Immovilli, F., Lorenzani, E., "Assessment of Master-Slave and Droop Control Strategies in Multi-Three-Phase Drives", IEEE Workshop on Electrical Machines Design, Control and Diagnosis (WEMDCD), pp. 163-168, 2021.

[4] Chen, B., Lv, J., Jiang, X., "Simplified Model Predictive Control of a Twelve-Phase Permanent Magnet Synchronous Motor", 45th Annual Conference of the IEEE Industrial Electronics Society (IECON), Vol. 1, 2019.

[5] Mingqing, Y., Hongwei, M., Jingpan, R., "Research on Control Strategy of Diode Clamped Three-Level 12-Phase Permanent Magnet Synchronous Motor", Chinese Automation Congress (CAC), pp. 3352-3357, 2020.

[6] Park, H., Kim, T., Suh, Y., "Fault-Tolerant Control Methods for Reduced Torque Ripple of Multiphase BLDC Motor Drive System Under Open-Circuit Faults", IEEE Trans. on Industry Applications, vol. 58, no. 6, pp. 7275-7285, 2022.

[7] Chen, B., Jiang, X., Lv, J., Chai, J., Zhang, X., Sheng, S., "A Decoupled Model Predictive Control Method for Twelve-Phase Permanent Magnet Synchronous Motors", IEEE Applied Power Electronics Conference and Exposition (APEC), 2020.

[8] Zhu, Z., Wang, S., Shao, B., Yan, L., Xu P., Ren, Y., "Advances in Dual-Three-Phase Permanent Magnet Synchronous Machines and Control Techniques", Energies, 2021.

[9] L.R. Rocha, E.C. Silva, P.H.A. Silva, G.X. Prestes, B.C.R. Cordeiro, L.F. Pessoa, R.P. Vieira, "Evaluation Methodology of Current Control Techniques for Torque Ripple Reduction in Non-Sinusoidal PMSM", IEEE 8th Southern Power Electronics Conference (SPEC), 2023.

[10] M.J. Nam, J.H. Kim, K.Y. Cho, H.W. Kim, Y. Cho, "Torque Ripple Reduction of an Interior PM Synchronous Motor by Compensating Harmonic Currents Based on Flux Linkage Harmonics", Journal of Power Electronics, vol. 17, no. 5, pp. 1223-1230, 2017.

[11] S. Mu, J. Kang, Z. Zhong, Z. Ma, "Improved detecting method for multiple rotating reference frames based harmonic control of PMSMs", Chinese Automation Congress (CAC), pp. 5458-5463, pp. 2020.

[12] J. Taylor, D.F. Valencia Garcia, W. Taha, M. Mohamadian, "Dynamic Modelling of Multiphase Machines Based on the VSD Transformation," SAE Technical Paper 2021-01-0774, doi:10.4271/2021-01-0774, 2021.

[13] Halvaei Niasar, A., Ahmadi, M., Edjtahed, S. H., "Sensorless Control of Non-Sinusoidal Permanent Magnet Brushless Motor Using Selective Torque Harmonic Elimination Control Method Based on Full-Order Sliding Mode Observer", Advances in Power Electronics Journal, vol. 2016, no. 9358604, pp. 1-13, 2016.

[14] Feng, G., Lai, C., Kelly, M., Kar, C., "Dual Three-Phase PMSM Torque Modeling and Maximum Torque per Peak Current Control Through Optimized Harmonic Current Injection", IEEE Trans. on Industrial Electronics, vol. 66, no. 5, pp. 3356-3368, 2019.

[15] H. Ghanayem, M. Alathamneh, R.M. Nelms, "A Comparative Study of PMSM Torque Control using Proportional-Integral and Proportional-Resonant Controllers", IEEE SoutheastCon, pp. 453-458, 2022.

[16] F. Hans, W. Schumacher, S. F. Chou, X. Wang, "Design of Multi frequency Proportional–Resonant Current Controllers for Voltage-Source Converters", IEEE Trans. on Power Electronics, vol. 35, no. 12, pp. 13573-13589, 2020.

[17] M. Fliess and C. Join, "Model-free control," International Journal of Control, vol. 86, no. 12, pp. 2228–2252, 2013.

[18] Y. Zhang, J. Jin, L. Huang, "Model-free predictive current control of PMSM drives based on extended state observer using ultralocal model", IEEE Trans. on Industrial Electronics, vol. 68, no. 2, pp. 993–1003, 2020.

[19] L. Zixuan, H. Xiaoyan, H. Qichao, G. Yang, Y. Wang, J. Shen, "Model-Free Predictive Current Control of PMSM Using Modified Extended State Observer", IEEE Trans. on Power Electronics, (Early Access), pp. 1-12, 2024.